INTERNATIONAL JOURNAL OF PRECISION ENGINEERING AND MANUFACTURING Vol. 17, No. 2, pp. 217-223 FEBRUARY 2016 / 217
DOI: 10.1007/s12541-016-0028-6 ISSN 2234-7593 (Print) / ISSN 2005-4602 (Online)

Incremental Forming of 3D Structured Aluminum Sheet

Van-Cuong Do[1], Duc-Toan Nguyen[2], Jun-Haeng Cho[3], and Young-Suk Kim[1,#]

1 School of Mechanical Engineering, Kyungpook National University, 80, Daehak-ro, Buk-gu, Daegu, 41566, South Korea
2 School of Mechanical Engineering, Hanoi University of Science and Technology, 1A Dai Co Viet Street, Hai Ba Trung District, Hanoi City, Vietnam
3 SEWON R&D Center, 554 Dalseo-ro, Dalseo-gu, Daegu, 42702, South Korea
Corresponding Author / E-mail: caekim@knu.ac.kr, TEL: +82-53-950-5580, FAX: +82-53-956-9914

KEYWORDS: Single point incremental forming (SPIF), 3D structured aluminum sheet (embossing)

In this paper we investigated the deformation characteristic of embossed aluminum sheet in the incremental sheet forming process which has frequently used in the design verification and the trial manufacturing of sheet products. The single point incremental forming (SPIF) experiments for the rectangular cone forming using the CNC machine with a chemical wood-machined die and a circular tool shape showed that the formability of the embossed sheet are better than that of the flat sheet in view of the maximum angle of cone forming. This comes from the fact that the embossed sheet between the tool and the elastic die wall is plastically compressed and the flatted area contributes to increase the plastic deformation. Also the tool path along the outward movement from the center showed a better formability than that of the inward movement from the edge. However the surface quality for the tool path along the outward movement evaluated from the surface deflection is inferior than that of the tool path along the inward movement. The experimental results and detail forming mechanism of the 3D structured sheet in incremental forming were reviewed with a finite element simulation using ABAQUS software.

Manuscript received: April 15, 2015 / Revised: September 14, 2015 / Accepted: September 23, 2015
This paper was presented at ISGMA 2015

1. Introduction

Recently, the automotive industry has made many efforts concentrated on lightweight materials to reduce fuel consumption as well as to enhance global environment protection. Aluminum and aluminum alloy have been selectively applied as interior and exterior automotive parts because of reduced weight and good working function.[1]

Among them, a three-dimensional (3D) structured heat shield of the engine exhaust system at a high temperature is widely used (Fig. 1). The embossed aluminum shield shows a very good heat dissipation effect because of the increased surface area. In addition, the flexural rigidity (stiffness reinforcement) is increased by the work hardening effect due to plastic deformation in the rolling process of the additional 3D structure (strain hardening effect). However, due to the 3D structure inherent in shape forming, the results show many limitations.[3,4]

Results to date show changes in the mechanical properties of the 3D structure according to the embossing depth of the embossed panel[5] and a study of deep-drawing formability, such as under typical deformation mode[6] or a few case studies on the actual panel.[7]

Recently, small-scale prototypes (trial product) using incremental sheet forming (ISF) technology by CNC machines for the quality assessment of the designs of new products in the automotive panel have been widely conducted.[8-10] Single Point Incremental Forming (SPIF) does not use the upper and lower dies, as in the conventional press-forming step. Instead, one or more spherical tools are mounted in the CNC machine to press the sheet material to form locally the desired product shape. Process parameters for forming the quality product include forming angle, tool size, machining pitch, tool path, and tool speed. An evaluation of the impacts[11] and the optimal tool path obtained,[12,13] two contact points in two-point incremental forming (TPIF);[14] in the case of material processing such as Ti4Al6V, a hybrid technique using a heating source,[15,16] and the springback in the ISF

Fig. 1 Application of embossed panels for heat protection

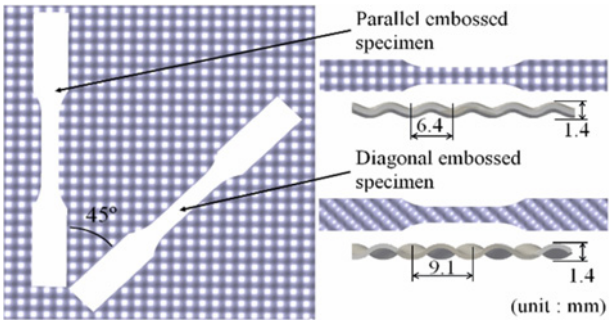

Fig. 2 Schematic of the cone-shaped embossing sheet

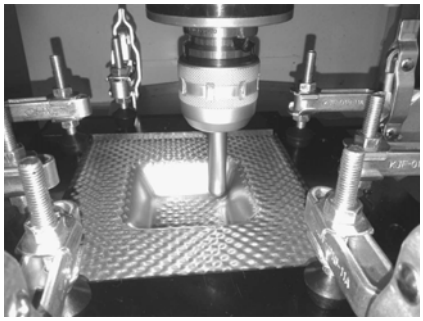

Fig. 3 CNC-based incremental forming machine using cylindrical tool and toggle clamp jig

Table 1 Mechanical properties for flat and embossed Al3004-P specimens evaluated by $\sigma = K\varepsilon^n$

	Flat Al3004-P	Embossed Al3004-P	
Direction	Mean	Parallel	Diagonal
Yield stress [MPa]	60.5	57.4	64.0
Tensile stregnth [MPa]	183	193	184
E [GPa]	70.0	47.0	58.3
Strain hardening Exponent, n	0.30	0.32	0.27
Strength coefficient K [MPa]	312	317	296
Elongation [%]	20	27	21
Plastic anisotropic Coefficient, R	0.59	0.03	0.23

evaluation[17-19] were implemented.

This paper is a basic research to develop a prototype of an embossed aluminum heat protector. The formability and springback characteristics of an embossed aluminum panel in the SPIF for the rectangular cone forming are evaluated and compared with the results of the original plain specimen. In addition, the effect of the tool path on the forming process is evaluated.

2. Incremental Forming of 3D Structured Aluminum Sheet

2.1 Material properties

Material used in this study includes Al3004-P aluminum sheet with the thickness of 0.51 mm. The embossing process is done by rolling the flat aluminum sheet between two embossed rollers with an embossed cone-shaped arrangement pitch of 6.4 mm and height of 0.7 mm. Uniaxial tension tests were conducted to measure the true stress-strain curves and the Lankford anisotropic parameters, R-values. The embossed aluminum sheet showed better mechanical properties compared to a plat aluminum sheet.[4]

2.2 Single point incremental forming experiments

Incremental forming using a single tool is referred to as SPIF. The appearance of the CNC machine tool and SPIF specimen used in the experiment are shown in Fig. 3.

The size of the specimen is 180 mm * 180 mm, the size of the die inlet is 80 mm * 80 mm, and the die shoulder radius is 10 mm. The

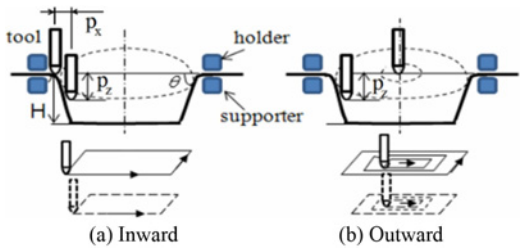

Fig. 4 Schematic view of the SPIF process for two tool paths: (a) inward movement of tool path, (b) outward movement of tool path

Table 2 Maximum forming angle for flat and embossed specimens

		Maximum formable angle (°)			
		60	62	64	66
Flat sheet		o	x		
Embossed sheet	Inward path	o	o	x	
	Outward path	o	o	o	x

o: Safe forming, x: failure occurred

diameter of the tool is 12 mm; the feed rate of the tool is 500 mm/min; the rotational speed of the tool is 2 rpm; the vertical pitch of the tool is 0.5 mm and the depth of formed shape is 50 mm. Applying a sufficient lubricant to the top of the sample before the experiment minimized the friction between the tool and the specimen. In addition, the outer boundary of the specimen (outer perimeter) is strongly pressed during the forming process.

With the same machining parameters, the forming angle increases from 60 degrees for the flat specimen to 62 degrees for the embossed specimen in the case of the same inward tool path. On the other hand, the maximum forming angle is improved from 62 degrees for the inward tool path to 64 degrees for the outward tool path with the same embossed specimens and the same machining parameters. The results are summarized in Table 2.

The entire surface of the square cone without fracture is bent inwardly. Springback occurred during progressive forming processes that did not use the lower die. When the tool moved the outer periphery of the cone section, it deformed the sheet through stretching and shear. The shear is parallel to the tool movement and increasing in the sheet cross section caused more deflection. The study of springback prediction

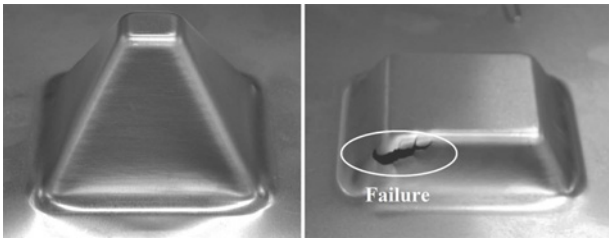

Fig. 5 Deformed shapes of flat specimen for the cone angles $\theta = 60°$ (safe formed, left) and 62° (failure occurred)

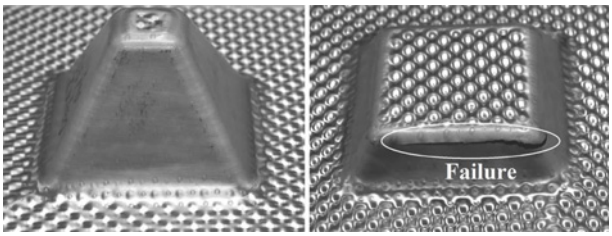

Fig. 6 (a) Deformed shapes of the embossed specimen for the cone angles $\theta = 62°$ (safe formed, left) and 64° (failure occurred, right) in the case of an inward movement tool path

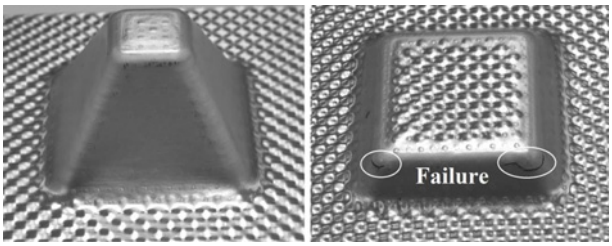

Fig. 6 (b) Deformed shapes of the embossed specimen for the cone angles $\theta = 64°$ (safe formed, left) and 66° (failure occurred, right) in the case of an outward movement tool path

and compensation for the embossed aluminum sheet will be left in further study.

From the incremental forming results, it can be seen that the embossed specimens exhibit a higher forming angle. This is explained by the increase in the plastic deformation when the tool presses the ridge and valley of the embossing plate (restoration).

On the other hand, the same embossed plate with the outward tool path could be formed at a greater angle than the inward tool path. This is the case of the outward tool path, as shown in Fig. 6, in that it gradually starts as the tool is moved to the outer circumference of the product from the center of the product. The tool is already formed so there is a large thickness difference in the entire working surface between the two tool path strategies. With the outward tool path, the forming sheet exhibits a greater plastic deformation in the previous steps. Additionally, for inward forming, due to the thickness difference between the tool center position and the formed section, the forming resistance at the tool center is increased, which is determined to cause

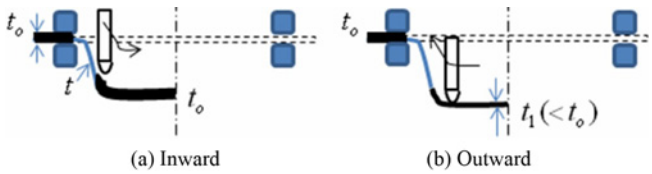

Fig. 7 Explanation of the difference of forming characteristics of embossed specimens between two tool paths, where t_0 is the original thickness, t is the deformed thickness at the cone-wall area, and t_1 is the deformed thickness at the cone-bottom area

a fracture at the formed area.

Jeswiet[20] presented that a maximum forming angle θ_{max} without fracture occurs for AA3003-O plate in the following equation.

$$\theta_{max} = 8.5t_0 + 60.7^0 \quad (1)$$

Where t_0 is the original thickness of the sheet with the unit of mm. If a 0.51-mm thick sheet is used in this study, the maximum forming angle is 65.035°. However, the results obtained in this study show there is actually a range between 60° and 64°. This error is determined to be due to the configuration and processing conditions of the products formed.

A cross section can be cut by the Wire Electric Discharge Machine to measure the cross section shape of the formed cones. A curved deflection surface to the inside showed that the occurrence of the springback in the wall area implies the formed products in Fig. 8(a). Each of the deflections is 2.80 mm, with 1.76 mm for the outward and inward toolpaths with embossed material, and 1.98 mm in the case of flat material.

Fig. 8(a), (b) show the thickness distribution in the gradient of the square cross-sectional shape and the forming angle of 60° do not cause a fracture in all cases.

Meanwhile, the thickness is greatly reduced through the cross-section, as shown in Fig. 8(b). At the position of about 20 mm from the bottom of the rectangular cone, the maximum thickness reduction ratio of the flat specimen is 56.47%, and for the embossed specimen with inward forming and outward forming, the ratios were 56.86% and 60.78%, respectively. In the case of outward forming, the material at the bottom of the cone shape is approximately 18.03% thinner.

The strain distribution of the flat specimen with a forming angle of 60° and different forming depths of 30 mm and 50 mm is shown in Fig. 9. The SPIF specimen is printed a grid plate with a diameter of 2.54 mm to analyze the strain. The strain of the deformed grids lied on the symmetric cross section A-A was measured after forming. The forming limit curve (FLC) is expressed with the forming limit curve at fracture (FLCF) that was derived using a program developed by the researchers.[21,22]

The forming limit at fracture is represented by

$$\varepsilon_1 = -\varepsilon_2 + b \quad (2)$$

Where ε_1 and ε_2 are major and minor strain respectively. To define b, as shown in Fig. 5, the fracture occurred at the depth of 16 mm by

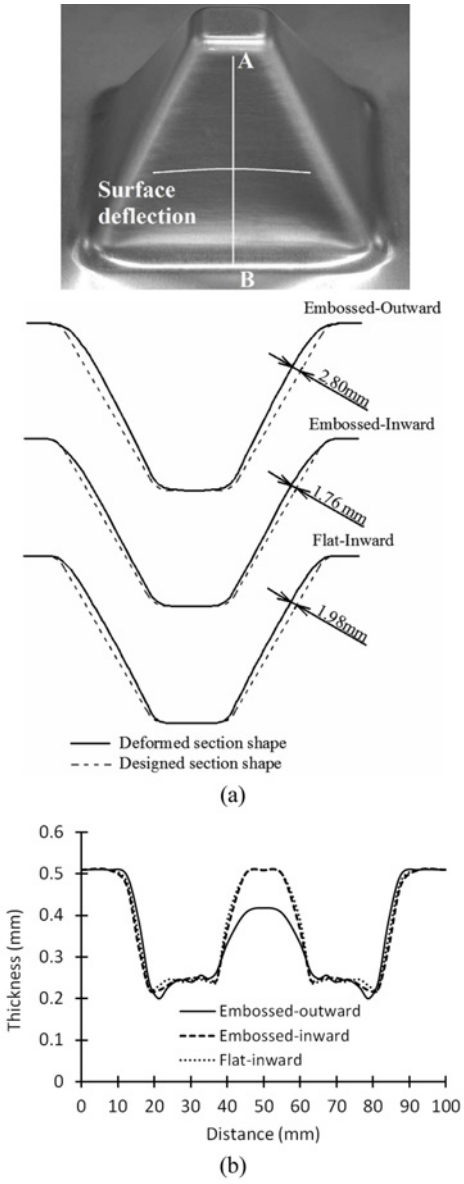

Fig. 8 (a) Cross-section view of deformed shape, (b) Thickness distribution along the section line AB for the flat specimen and the two embossed specimens at the cone angle $\theta = 60°$

experiment. The single point incremental forming process of the same-size truncated pyramidal shape with the wall angle of 62 degree is simulated by ABAQUS/Explicit finite element code to see the strain evolution at the corner of the pyramid where it is considered as equi-biaxial tension ($\varepsilon_1 = \varepsilon_2$). At the depth of 16 mm, the strain reached the value of 0.71. Then substituting this values to the Eq. (2), the value of b was obtained as 1.42.

As shown in Fig. 9, the minor strain is from 0 to 0.1. The forming process of the square cone is considered a substantially plain strain. In addition, the strain distribution is seen to be under the FLC at fracture. No fracture occurred.

In the case of the embossed material, strain measurement is difficult. This study does not compare the surface of the experimental shape and the FLC at fracture.

In the square cone forming without a lower die of this study, the

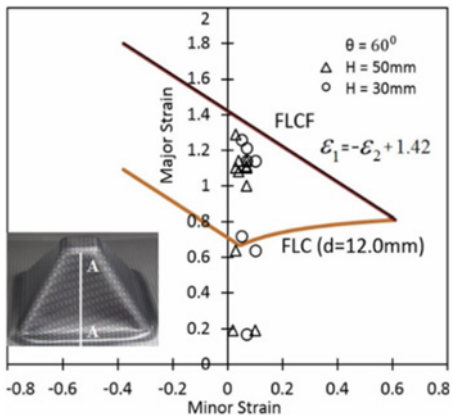

Fig. 9 The strain distribution and forming severity evaluated using forming limit curve at fracture of the flat specimen

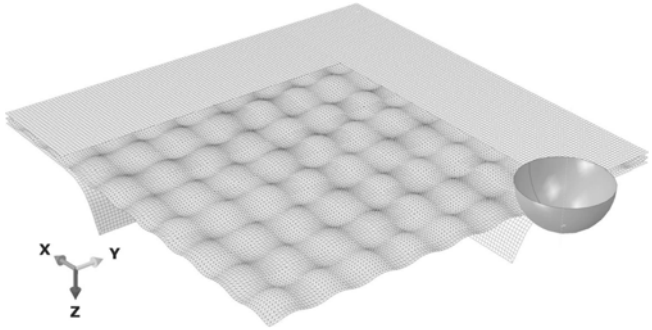

Fig. 10 Finite Element Model for embossed aluminum sheet SPIF

outward tool path is able to form at a greater forming angle and deflection compared to the inward tool path. This result conflicts with the study of Kitazawa[23] in that the outward tool path showed a better surface quality than the inward tool path.

2.3 Finite element simulation

In this study, the commercial ABAQUS/Explicit finite element code is used to simulate the SPIF process. This software gives elastic-plastic and rigid-plastic simulations of metal forming for large deformations. The elastic-plastic simulation is used; material density is 2.7E-9 ton/mm^3; Young modulus is 47 GPa; Poisson ratio is 0.3; the stress-strain curve is evaluated by $\sigma = K\varepsilon^n$ with strength coefficient (K) of 317 MPa and strain hardening coefficient (n) of 0.32.

Fig. 10 shows the finite element model for the incremental sheet forming process of a square cone with an embossed sheet. Only the quarter model is considered to reduce the simulation time but it ensured the correct results because of the symmetry condition. The embossed specimen size is 60 × 60 mm^2 and the size of square cone is 40 × 40 mm^2. The depth is 30 mm with the increment is 1 mm and the wall angle is 60°.

The tool with diameter 12 mm is analytically rigid. The die and holder are discretely rigid and meshed by the R3D4 element. The embossed sheet is drawn by the CATIA software and imported to ABAQUS explicit. The element for the embossed sheet is a triangle shape, S4R

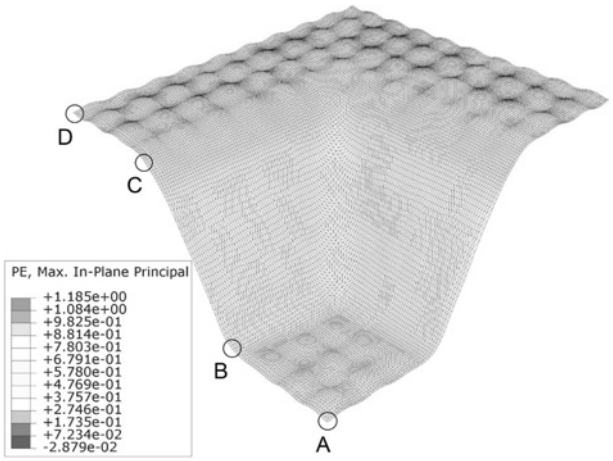

Fig. 11 The formed shape and plastic strain in simulation

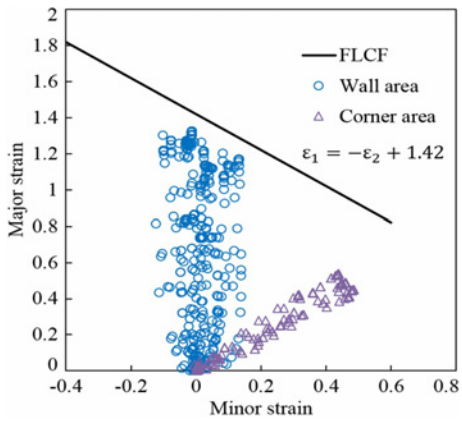

Fig. 12 The plastic strain evolution in the wall area and corner area of the pyramidal shape

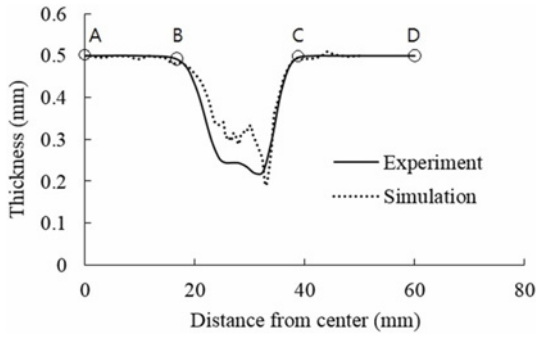

Fig. 13 The thickness distribution by experimental data and simulation data

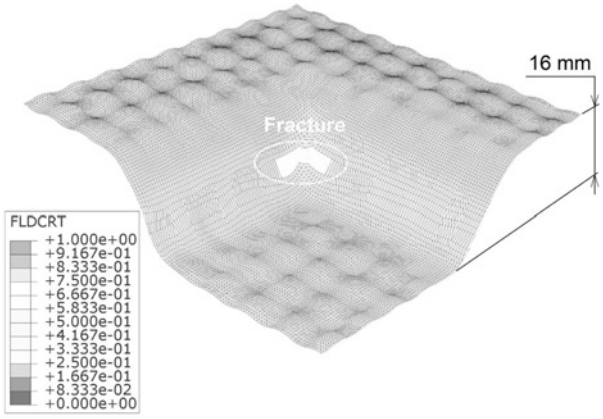

Fig. 14 Fracture occurs in the case of forming angle of 64 degree

type, size 0.5 mm, and five points through thickness in Gauss integration.

The speed in this simulation is about 80 mm/s as similar as the speed in the experiment. To reduce the simulation time, mass scaling is applied but it still remains the kinetic energy of deforming material less than 10% of total energy of the system in order to reduce the effect of vibration on the simulation accuracy. The mass scaling value of 100 times is used in this simulation. The computer is used in the simulation with the processor Intel(R) core TM i7 2.8 GHz and installed memory (RAM) of 16.0 GB. The simulation time is approximately 72 hours.

In the blank area (from C to D) and the bottom area (from A to B), the plastic strain is nearly zero and the thickness keeps the same at initial value. In Fig. 12, the maximum major strain is 1.32 and the value on the FLCF is 1.56 at the same minor strain. In Fig. 13, the simulation thickness decreases dramatically in the wall area (from B to C) and gets to a peak at the distance about 30 mm from the center of the part. At this position, the experiment thickness of the parts is also minimum. This is the reason for the failures that always occur at the same position for the parts with different shape structures and tool paths, as mentioned in Figs. 5 and 6. In detail, the minimum thickness in experiment is 0.22 mm and in simulation is 0.19 mm. The difference in thickness distribution between experiment and simulation comes from some reasons. Firstly, the simulation includes only SPIF process that the emboss sheet is drawn by CATIA software and converted into shell part in ABAQUS with the constant initial thickness. This is not similar to actual embossed sheet with plastic deformation after embossing process. Secondly, the material property for embossed sheet is isotropic in simulation. It does not describe the local hardening caused by previous process. This will be implemented in next research.

In order to verify the ductile fracture criterion based on FLC failure criterion, FLC data obtained from previous results were implemented into ABAQUS/Explicit to simulate the forming process. Here, when the FLC failure criterion at an element, which was defined by the ratio of the major strain and the FLC value at the same point for the minor strains, reaches to unit value. Then the fracture area could be deleted following softening behavior of damage model or remained to see the evolution of failure.

The simulation was done with the forming angle of 64 degree. The FE simulation results for critical test samples are presented Fig. 14. Here, FLC ductile fracture value (FLDCRT) approached 1.0 (the condition of failure) then the fracture occurs and maximum deformed height was obtained for corresponding wall angles. The results shows that the fracture occurs at the similar depth in comparison with experiment.

3. Conclusions

This study investigated the characteristics of 3D structured aluminum panels (embossed panels) by SPIF, which is widely used in automotive exhaust products.

Through a comparison with the original plain Aluminum 3004-P sheet with the inward tool path, the results showed the embossed sheet exhibits a better forming angle and part accuracy. This is the result of a previous rolling process to make the embossed aluminum sheet, which created local hardening and plastic deformation. Furthermore, the tool in the CNC presses the ridge and valley of the embossed sheet during the SPIF process, and the restoration increases the plastic deformation of the material. Additionally, with the outward tool path, the embossed sheet showed improved formability because of the increased deformable section and reduced forming resistance.

Furthermore, the Finite Element simulation by ABAQUS software analyzed the plastic strain that is very difficult to measure by actual experiment for embossed specimen. The thickness distribution result is quite similar to experimental data. The simulation accuracy can be improved by describing the previous local hardening and plastic deformation in material before SPIF process.

The incremental forming process did not use a lower die and a finite element analysis for compensating prediction studies is on its way.

ACKNOWLEDGEMENT

This work was supported by the National Research Foundation of Korea (NRF) grant funded by the Korea government (MEST) (NRF-2014R1A2A2A01005903)

REFERENCES

1. Kim, Y. S., Kim, K. S., and Kwon, N. C., “Press Formabilities of Aluminum Sheets for Autobody Application,” Proc. of the KSAE Conference, pp. 233-246, 1993.
2. Kim, Y. S., “Evaluation Apparatus and Method for Insulation Efficiency of the Heat Protector of the Automobile,” KR Patent, No. 10-1004202, 2010.
3. Arcelor Mittal, “Steels Coated with Alusi Aluminum-Silicon Alloy: Specific Applications,” http://automotive.arcelormittal.com/europe/products/alusi/alusi_specific_applications/EN (Accessed 24 DEC 2015)
4. Kim, Y. S., Cho, J. H., Do, V. C, and Shin, D. W, “Evaluation of Mechanical Properties and Springback for 3D-Structured Aluminum Sheet - Part I,” Journal of the Korea Academia-Industrial Cooperation Society, Vol. 16, No. 2, pp. 921-926, 2015.
5. Güler, H. and Özcan, R., “Effects of the Rotary Embossing Process on Mechanical Properties in Aluminum Alloy 1050 Sheet,” Metals and Materials International, Vol. 18, No. 2, pp. 225-230, 2012.
6. Abe, T., Yasota, T., Nonaka, Y., Saka, S., Kuwabara, T., “Forming Simulation of Emboss Formation by Roll Forming,” Proc. of Japanese Spring Conference for the Technology Plasticity, pp.253-254, 2008
7. Melnykowycz, M. and Caprioli, D., “Development of Aluminum Heat Shield Designs using OptiStruct and HyperForm,” Proc. of 4th European HyperWorks Technology Conference, 2010.
8. Iseki, H., Kato, K., and Sakamoto, S., “Flexible and Incremental Sheet Metal Bulging using a Path-Controlled Spherical Roller,” Transactions of JSME-C, Vol. 58, No. 554, pp. 3147-3155, 1992.
9. Emmens, W. C., Sebastiani, G., and Van den Boogaard, A., “The Technology of Incremental Sheet Forming-A Brief Review of the History,” Journal of Materials Processing Technology, Vol. 210, No. 8, pp. 981-997, 2010.
10. Jeswiet, J., Micari, F., Hirt, G., Bramley, A., Duflou, J., and Allwood, J., “Asymmetric Single Point Incremental Forming of Sheet Metal,” CIRP Annals-Manufacturing Technology, Vol. 54, No. 2, pp. 88-114, 2005.
11. Kim, Y. H. and Park, J. J., “Effect of Process Parameters on Formability in Incremental Forming of Sheet Metal,” Journal of Materials Processing Technology, Vols. 130-131, pp. 42-46, 2002.
12. Kim, T. J. and Yang, D. Y., “Improvement of Formability for the Incremental Sheet Metal Forming Process,” International Journal of Mechanical Sciences, Vol. 42, No. 7, pp. 1271-1286, 2000.
13. Azaouzi, M. and Lebaal, N., “Tool Path Optimization for Single Point Incremental Sheet Forming using Response Surface Method,” Simulation Modelling Practice and Theory, Vol. 24, pp. 49-58, 2012.
14. Jackson, K. and Allwood, J., “The Mechanics of Incremental Sheet Forming,” Journal of Materials Processing Technology, Vol. 209, No. 3, pp. 1158-1174, 2009.
15. Araghi, B. T., Göttmann, A., Bambach, M., Hirt, G., Bergweiler, G., et al., “Review on the Development of a Hybrid Incremental Sheet Forming System for Small Batch Sizes and Individualized Production,” Production Engineering, Vol. 5, No. 4, pp. 393-404, 2011.
16. Göttmann, A., Diettrich, J., Bergweiler, G., Bambach, M., Hirt, G., et al., “Laser-Assisted Asymmetric Incremental Sheet Forming of Titanium Sheet Metal Parts,” Production Engineering, Vol. 5, No. 3, pp. 263-271, 2011.
17. Fei, H., Mo, J.-H., Qi, H.-W., Long, R.-F., Cui, X.-H., and Li, Z.-W., “Springback Prediction for Incremental Sheet Forming based on FEM-PSONN Technology,” Transactions of Nonferrous Metals Society of China, Vol. 23, No. 4, pp. 1061-1071, 2013.
18. Zettler, J., Rezai, H., and Hirt, G., “Springback Compensation for Incremental Sheet Metal Forming Applications,” Proc. of LS-DYNA Anwenderforum, C-I-21-C-I-32, 2008.
19. Khan, M. S., Coenen, F., Dixon, C., El-Salhi, S., Penalva, M., and Rivero, A., “An Intelligent Process Model: Predicting Springback in Single Point Incremental Forming,” The International Journal of

Advanced Manufacturing Technology, Vol. 76, No. 9-12, pp. 2071-2082, 2015.

20. Jeswiet, J., Hagan, E., and Szekeres, A., "Forming Parameters For Incremental Forming of Aluminium Alloy Sheet Metal," Journal of Engineering Manufacture, Vol. 216, No. 10, pp. 1367-1371, 2002.

21. Nguyen, D.-T. and Kim, Y.-S., "A Numerical Study on Establishing the Forming Limit Curve and Indicating the Formability of Complex Shape in Incremental Sheet Forming Process," Int. J. Precis. Eng. Manuf., Vol. 14, No. 12, pp. 2087-2093, 2013.

22. Nguyen, D. T., Yang, S. H., Jung, D. W., Choi, T. H., and Kim, Y. S., "Incremental Sheet Metal Forming: Numerical Simulation and Rapid Prototyping Process to Make an Automobile White-Body," Steel Research International, Vol. 82, No. 7, pp. 795-805, 2011.

23. Kitazawa, K., Wakabayashi, A., Murata, K., and Yaejima, K., "Metal-Flow Phenomena in Computerized Numerically Controlled Incremental Stretch-Expanding of Aluminum Sheets," Japan Institute of Light Metals, Journal, Vol. 46, No. 2, pp. 65-70, 1996.